Check for updates

ADVANCED ENERGY MATERIALS
www.advenergymat.de

An Aqueous Rechargeable Al-Ion Battery Based on Cobalt Hexacyanoferrate and Al Metal

Xinhai Yuan, Xuelong Yuan, Shuaishuai Zhang, Peng Chen, Xiongwei Wu, Jilei Ye, Lili Liu, Lijun Fu, Tao Wang, Kenneth I. Ozoemena,* and Yuping Wu**

Like other aqueous batteries, aqueous rechargeable Al-ion batteries (ARAIBs) have attracted much attention due to their high safety and low cost. However, the low energy density of ARAIBs limits its popularization and application. In order to solve this problem, in addition to choosing Al metal as the negative electrode, it is also necessary to choose a suitable positive electrode material. Here, a cubic phase cobalt hexacyanoferrate (CoHCF) with excellent rate and cycling performance is used as the positive electrode material. Due to the reversible catalysis of the Cl^-/Cl^0 reaction at high potential in saturated $AlCl_3$ solution, it has the characteristics of high capacity up to 103.5 mAh g^{-1}. Combined with the Al metal as negative electrode, an ARAIB with an average discharge voltage of 1.56 V and an energy density of 155 Wh kg^{-1} is constructed, which shows outstanding cycling and rate performances.

1. Introduction

In response to the continually rising energy demands, innovative energy storage systems, exemplified by aluminum-ion batteries with their rapid charging capabilities, extended cycle life, and significant capacity, are increasingly being recognized as one of the most promising solutions for next-generation energy storage.[1–5] Due to its low relative atomic mass and the three-electron transfer process in the redox process, Al possesses of high mass and volume-specific capacities, and its volume-specific capacity is even higher than those of Li and Zn.[6–8] In addition, Al is abundant in resources, making it a cost-effective battery metal. However, most Al-ion batteries use ionic liquids (IL, such as [EMIM]Cl-$AlCl_3$) as electrolytes, which not only increases manufacturing costs, but also makes assembly conditions more stringent, which greatly limits their commercial applications.[1,9,10] Therefore, the development of aqueous rechargeable Al-ion batteries (ARAIBs) has received great attention. However, because of the low reduction potential of Al (−1.68 V vs SHE), hydrogen evolution reaction (HER) instead of aluminum deposition occurs on the Al electrode in an aqueous solution.[11–16] Hence, it is difficult to use Al metal as a negative electrode directly to build an ARAIB. In 2018, Zhao et al. introduced an IL-enriched film to the surface of Al by treating it in an acidic ionic liquid electrolyte ([EMIM]Cl-$AlCl_3$).[17] It was found that the treated Al (T-Al) can work reversibly in $Al(CF_3SO_3)_3$ aqueous electrolyte. Based on the modified aluminum negative electrode, T-Al//MnO_2 batteries with stable electrochemical performance were successfully assembled.[17,18] However, the low discharge platform (≈1.3 V) and the high price of $Al(CF_3SO_3)_3$ restricted its further development. In 2019, Pan

X. Yuan, X. Yuan, S. Zhang, J. Ye, L. Liu, L. Fu, Y. Wu
State Key Laboratory of Materials-Oriented Chemical Engineering School of Energy Science and Engineering
State Key Laboratory of Materials-Oriented Chemical Engineering
Nanjing Tech University
Nanjing, Jiangsu Province 211816, China
E-mail: l.fu@njtech.edu.cn; wuyp@seu.edu.cn

P. Chen
Key Laboratory for Ecological Metallurgy of Multimetallic Minerals (Ministry of Education)
School of Metallurgy
Northeastern University
Shenyang 110819, China

X. Wu
School of Chemistry and Materials Science
Hunan Agricultural University
Changsha 410128, China

T. Wang, Y. Wu
Confucius Energy Storage Lab
School of Energy and Environment
Southeast University
Nanjing, Jiangsu Province 210096, China

K. I. Ozoemena
Molecular Sciences Institute
School of Chemistry
University of the Witwatersrand
Private Bag 3, Wits, Johannesburg 2050, South Africa
E-mail: kenneth.ozoemena@wits.ac.za

The ORCID identification number(s) for the author(s) of this article can be found under https://doi.org/10.1002/aenm.202302712

DOI: 10.1002/aenm.202302712

 © 2023 Wiley-VCH GmbH

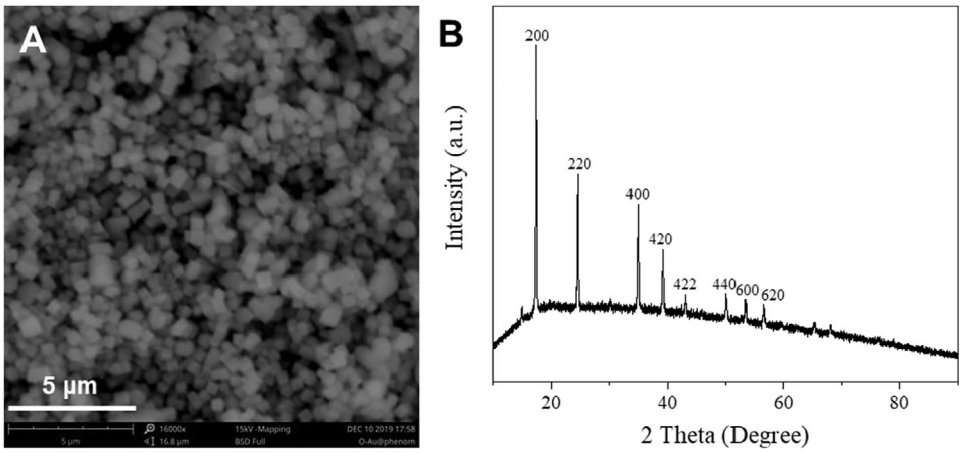

Figure 1. Some physical property characterization of CoHCF nanocubes: A) SEM image and B) XRD pattern.

et al found that the reversible deposition and stripping of aluminum can be realized in the ultra-concentrated aqueous solution of $AlCl_3 \cdot 6H_2O$. Then an aqueous rechargeable Al-graphite battery was successfully assembled, with an average discharge voltage of 1.44 V, an energy density of up to 220 Wh kg^{-1}, and shows excellent cycling performance.[11] This study not only indicates a new direction for the further development of ARAIBs, but also has great application value due to the use of low price $AlCl_3 \cdot 6H_2O$, which can greatly reduce the manufacturing cost of the battery.

In order to construct high energy density ARAIB, besides using Al metal as negative electrode, it is necessary to find suitable positive electrode materials. Although many materials have been studied, their performance is not satisfactory such as high voltage but low capacity,[19,20] high capacity but low voltage,[21,22] or poor cycling performance.[23] Here, we reported nanocube cobalt hexacyanoferrate (CoHCF) as a positive electrode material for ARAIBs. Based on this positive material and Al negative electrode, an ARAIB was constructed with an average discharge voltage of 1.56 V and an energy density of 155 Wh kg^{-1}. Moreover, this battery configuraion not only boasts a high energy density but also excels in rate performance and cycling stability, making it a promising candidate for advanced energy storage applications.

2. Results and Discussions

As shown in **Figure 1**A and Figure S1A (Supporting Information), the synthesized CoHCF is nanocube structure with a size of about 500 nm. The X-ray diffraction (XRD) analysis (Figure 1B) confirms the CoHCF sample is a cubic phase of the $Fm\bar{3}m$ space group with a typical open framework consisting of Co cation with N coordination and Fe cation with C coordination.[24,25] According to the results of inductively coupled plasma optical emission spectrometry (ICP-OES) (Table S1, Supporting Information) and thermogravimetric analysis (TG) (Figure S1B, Supporting Information), the composition of CoHCF is $KCoFe(CN)_6 \cdot 5.5H_2O$.

As shown in **Figure 2**, CoHCF exhibits excellent electrochemical properties in saturated $AlCl_3$ aqueous electrolyte (≈3 M). The potential range of single electrode test is set to − 0.2–1.1 V (vs SCE). The cyclic voltammetry (CV) results (Figure 2A) show that CoHCF has two pairs of redox peaks. Taking the CV curve at the scan rate of 1 mV s^{-1} as an example, two pairs of redox peaks are located at 0.497/0.33 V and 0.96/1.05 V (vs SCE), respectively. With an increasing scan rate, the distinction between the redox peaks grows more evident. Remarkably, even when the scan rate reaches 5 mV s^{-1}, the redox peaks are clearly discernible, implying that CoHCF could demonstrate outstanding rate capabilities, as illustrated in Figure 2B. When the current densities are 0.125, 0.25, 0.5, 0.75, 1, 1.5, 2, 2.5, 3, and 4 A g^{-1}, the specific discharge capacities are 103.5, 95.8, 88.2, 83.5, 79.9, 76.8, 72.9, 69.8, 68.1, and 65.6 mAh g^{-1}, respectively. Such excellent rate performance can be attributed to its open framework structure, which is conducive to the rapid insertion and de-insertion of ions.[26–28] In addition, it has a high average discharge potential (Figure 2C). When the current density is 0.125 A g^{-1}, the average discharge potential is 0.65 V (vs SCE). Even when the current density reaches 1 A g^{-1}, the average discharge potential is still as high as 0.6 V (vs SCE). Such a high average discharge potential will contribute to the construction of high-voltage ARAIB. Further study (Figure 2D) shows that CoHCF also exhibits excellent cycling performance, with a capacity retention of 97.5% after 1000 cycles at a current density of 0.25 A g^{-1}.

In an effort to explore the charge–discharge mechanism, we first carried out the characterization of ex-situ X-ray diffraction (XRD), and the results are shown in **Figure 3**A–C. Upon charging, the peak corresponding to (011) plane first moves to a lower angle, signifying the extraction of cations from the lattice of CoHCF.[29,30] The pH of a saturated aluminum chloride aqueous solution is 0.77, corresponding to a hydrogen ion concentration of $[H^+] \approx 1.7 \times 10^{-1}$ mol L^{-1}. The concentration of H^+ is significant, suggesting that H^+ might also be incorporated into the CoHCF lattice. When the operating voltage range is between −0.2 and 0.9 V, the discharge curve of the CoHCF electrode in 1.7×10^{-1} mol L^{-1} HCl solution is similar to its discharge curve in a saturated $AlCl_3$ aqueous solution (Figure S2, Supporting Information). Moreover, their capacities are closely matched. This indicates that H^+ can also be embedded in the CoHCF lattice. Does this mean that the incorporation of Al^{3+} is minimal or non-existent? To investigate this, we characterized CoHCF at its discharged state using ICP-OES and determined

© 2023 Wiley-VCH GmbH

16146840, 2024, 3, Downloaded from https://onlinelibrary.wiley.com/doi/10.1002/aenm.202302712 by University Of Witwatersrand, Wiley Online Library on [02/12/2024]. See the Terms and Conditions (https://onlinelibrary.wiley.com/terms-and-conditions) on Wiley Online Library for rules of use; OA articles are governed by the applicable Creative Commons License

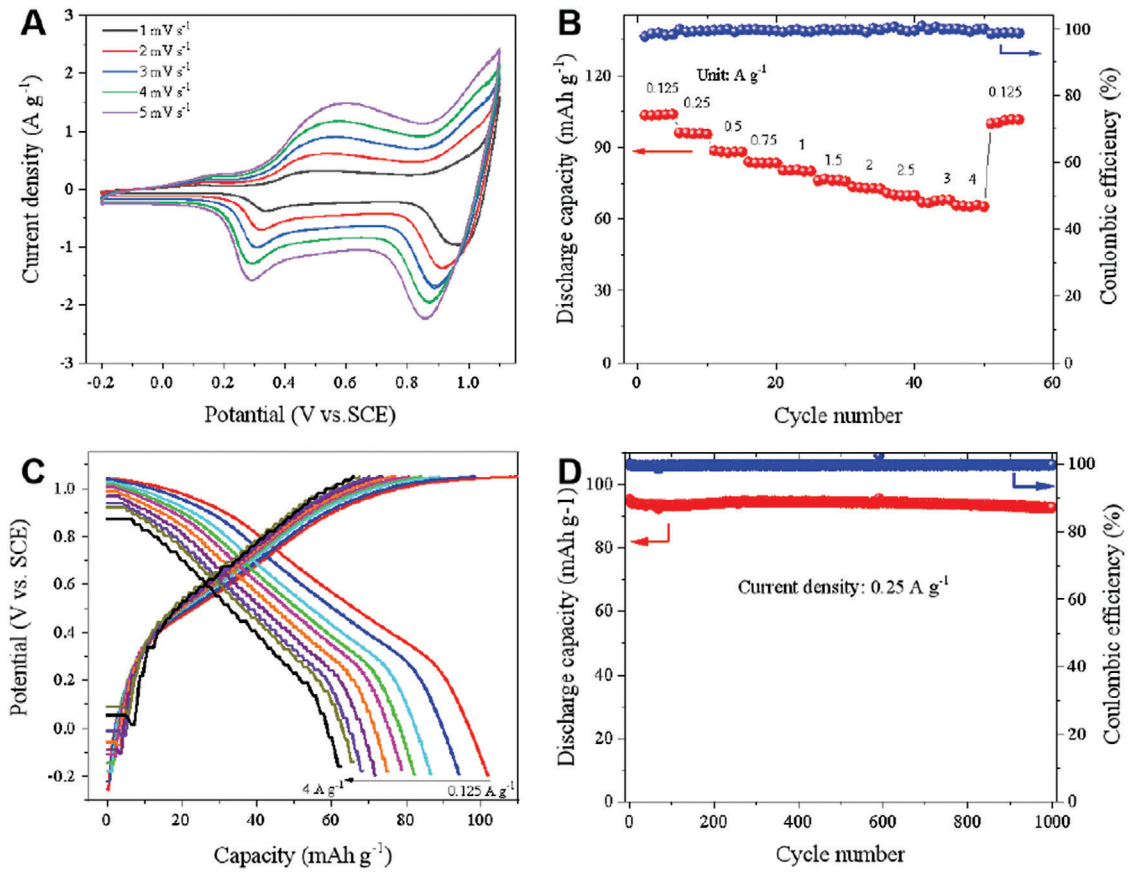

Figure 2. Characterization of the electrochemical properties of CoHCF electrode in saturated $AlCl_3$ aqueous electrolyte: A) CV curves at different scanning rates; B) cycling performance at different current densities; C) charge–discharge curves at different current densities; and D) cycling performance test at the current density of 0.25 A g^{-1}.

the contribution to its capacity based on the content of Al^{3+}. As shown in Table S2 (Supporting Information), the composition of the sample at the discharge termination state was found to be $CoFeAl_{0.254}(CN)_6 \cdot 5.5H_2O$. Based on the formula $Q = 26800*n/M$ ('n' represents the number of moles, and 'M' denotes the molar mass), the contribution to capacity from Al^{3+} incorporation is approximately 50 mAh g^{-1}. This suggests that in the presence of both Al^{3+} and H^+, they co-insert into the CoHCF lattice, with Al^{3+} being preferentially incorporated. It is interesting that when the potential reaches 1 V, the peak corresponding to (011) crystal plane (which is located at 17.41°) moves slightly to a higher angle (Figure 3C). This indicates that when the charging potential is higher than 0.9 V, ions or molecule may insert into the crystal lattice of CoHCF. The discharge process is opposite to the charging process, and the peak corresponding to (011) plane first moves to a low angle and then to a high one. This indicates that when the charging potential is higher than 0.9 V, ions or molecule may insert into the crystal lattice of CoHCF.

To explore the reaction mechanism of CoHCF electrode at high potential (above 0.9 V vs SCE) in the charging process, we took out the CoHCF electrode charged to 1.05 V, soaked it in ultrapure water for 1 h, then dried and analyzed the element composition with EDS (Figure S3, Supporting Information). A small amount of Cl elements was detected. Subsequently, we devised another experiment. Mirroring the previously described procedure, we charged the CoHCF electrode to 1.05 V (vs SCE), removed it, and immersed it in ultrapure water for 1 h, followed by a discharge test as illustrated in Figure S4 (Supporting Information). It is found that there is a specific capacity loss of 30 mAh g^{-1} in this process. From our understanding, when ions are embedded within the electrode material, they remain trapped and would not spontaneously release, even after immersion in pure water. This means that if Cl^- is incorporated at a high potential, a drastic capacity loss should not be observed after post-immersion. Hence, the most logical inference is that, under high potentials, the Cl element is adsorbed onto the CoHCF electrode. Yet, the question remains: in what form or state is the Cl element adsorbed on the CoHCF electrode? To delve deeper on this issue, XPS analysis on both the pristine CoHCF electrode and the one post-high voltage charging was carried out. As illustrated in Figure 3D, E, regardless of whether it is the pristine sample or the one after high-voltage charging, the valence state of the Co element remains at +2. Previous research shows that if ion intercalation or de-intercalation occurs in the CoHCF electrode during charge-discharge cycles, the capacity at lower potentials is associated with the Fe^{3+}/Fe^{2+} redox couple, while the capacity at higher potentials relates to the Co^{3+}/Co^{2+} redox couple.[24] However, it is noteworthy that after charging at high voltage, the Co^{2+}

© 2023 Wiley-VCH GmbH

16146840, 2024, 3, Downloaded from https://onlinelibrary.wiley.com/doi/10.1002/aenm.202302712 by University Of Witwatersrand, Wiley Online Library on [02/12/2024]. See the Terms and Conditions (https://onlinelibrary.wiley.com/terms-and-conditions) on Wiley Online Library for rules of use; OA articles are governed by the applicable Creative Commons License

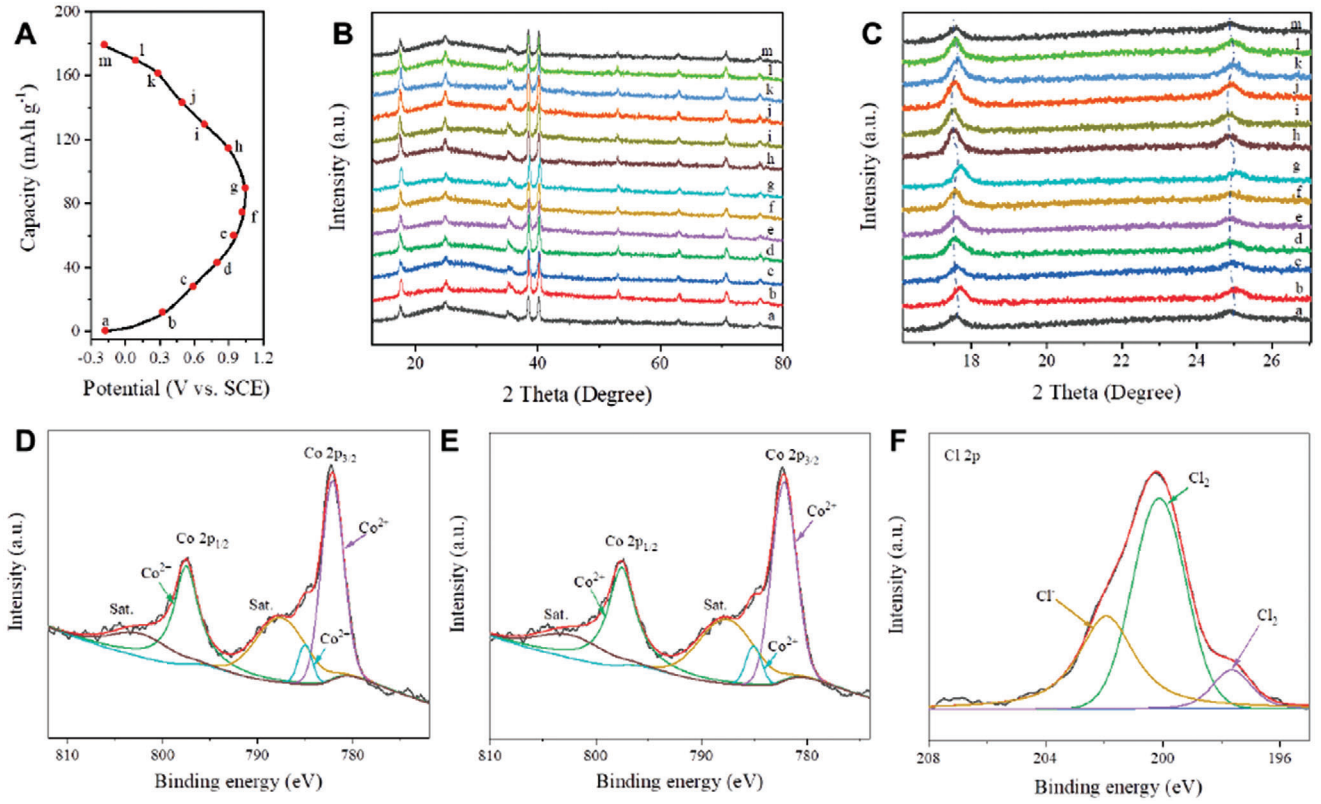

Figure 3. Study on the working mechanism of CoHCF electrode in saturated $AlCl_3$ aqueous electrolyte: A) Charge–discharge curve of CoHCF electrode at a current density of 0.25 A g^{-1}; B,C) ex situ XRD curves corresponding to electrodes in different charge-discharge states in Figure 3A; High resolution X-ray photoelectron spectra (XPS) of the Co $2p_{1/2}$ for the original CoHCF electrode D) and the charged CoHCF electrode at high potential; and E) high resolution XPS of the Cl 2p for the charged CoHCF electrode at high potential.

in the CoHCF electrode did not oxidize to Co^{3+}. This further confirms that at high potentials, Cl^- did not truly intercalate into the CoHCF electrode. The XPS results (Figure S2, Supporting Information) further indicate the presence of Cl^0 in the sample after charging at high voltage. According to the former reports,[31,32] Cl^-/Cl^0 redox pairs have a high potential and can also exhibit high reversibility in aqueous solutions. Therefore, we can determine that the oxidation reaction of Cl^- to Cl^0 occurs on the CoHCF electrode at high potential.

What role did the CoHCF electrode play in the above process? What effect does the composition of the solution have on the oxidation reaction of Cl^- to Cl^0? To understand these issues, we tested the electrochemical performance of CoHCF electrodes in different aqueous solutions. The findings reveal that the CV curve lacks a redox peak at high potential as depicted in Figure S5A (Supporting Information), and there is no oxidation–reduction plateau at high potential as illustrated in Figure S5B (Supporting Information) when in a saturated $Al_2(SO_4)_3$ solution. It has been proved that the insertion/de-insertion of Al^{3+}/H^+ occurred in CoHCF electrode during the charge discharge process in $Al_2(SO_4)_3$ solution. Therefore, this indicates that the specific capacity of reversible insertion/de-insertion of Al^{3+}/H^+ on CoHCF electrodes is only 52.4 mAh g^{-1}. The cycling test of CoHCF electrode in saturated $Al_2(SO_4)_3$ solution at a current density of 0.25 A g^{-1} is shown in Figure S5C (Supporting Information). After 1000 cycles, its capacity retention rate is 51.3%. The CoHCF electrode exhibits excellent cycling performance in saturated $AlCl_3$ solution in stark contrast to its cycling performance in saturated $Al_2(SO_4)_3$ solution. This indicates that $AlCl_3$ solution helps to improve the cycling stability of CoHCF electrodes. In 0.5 M $AlCl_3$ aqueous solution, a small platform appeared at high potential. It can be seen from the charge/discharge curve that the specific capacity in 0.5 M $AlCl_3$ aqueous solution is about 10 mAh g^{-1} higher than that in $Al_2(SO_4)_3$ solution, corresponding to the previous test results (Figure S4, Supporting Information). This shows that the platform at high potential in 0.5 M $AlCl_3$ aqueous solution corresponds to the redox of Cl^-/Cl^0 pair. When the concentration of $AlCl_3$ solution increased to 1 M, the redox peak at high potential began to become obvious and sharper. With the concentration increasing, the redox peak began to become wider. It can be seen from the charge/discharge curve (**Figure 4B**) that the charge/discharge specific capacity of the CoHCF electrode increases gradually with the concentration. The results of Raman test show that when the concentration of $AlCl_3$ solution increases to 2 M, $Al_2Cl_7^-$ appears in the solution; and when the concentration reaches saturation, the content of $Al_2Cl_7^-$ reaches the maximum value (Figure 4C). This shows that the increase of $Al_2Cl_7^-$ content is beneficial to the improvement of redox activity of Cl^-/Cl^0 pair. The cycling performance of CoHCF electrodes in different concentrations of $AlCl_3$ aqueous solutions is shown in Figure S6 (Supporting Information). Notably, as the concentration of $AlCl_3$ increases, there is a corresponding

© 2023 Wiley-VCH GmbH

16146840, 2024, 3, Downloaded from https://onlinelibrary.wiley.com/doi/10.1002/aenm.202302712 by University Of Witwatersrand, Wiley Online Library on [02/12/2024]. See the Terms and Conditions (https://onlinelibrary.wiley.com/terms-and-conditions) on Wiley Online Library for rules of use; OA articles are governed by the applicable Creative Commons License

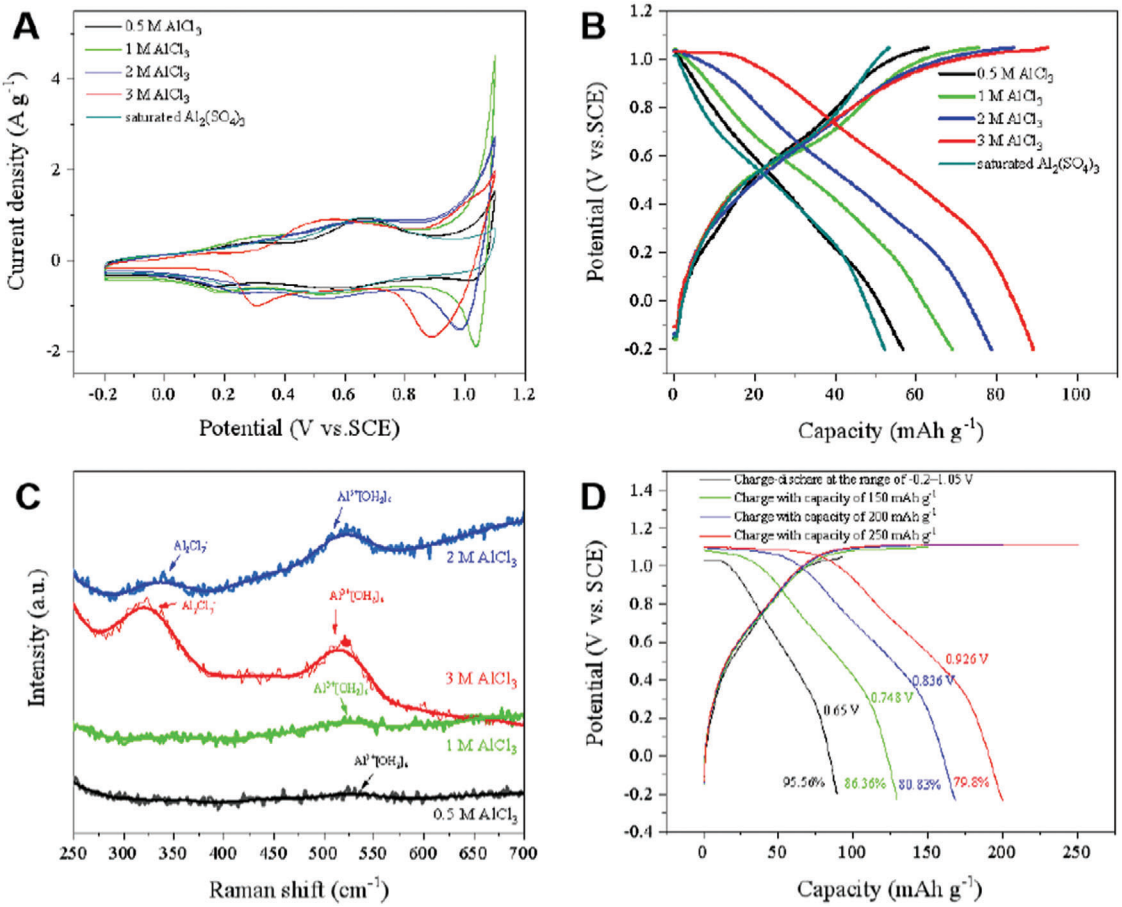

Figure 4. Electrochemical performance of CoHCF electrode in different aqueous electrolytes: A) Circulating voltammetry test of CoHCF electrode in different electrolyte (3 mV s^{-1}); B) the charge–discharge curve of CoHCF electrode at the current density of 0.25 A g^{-1} in different electrolyte; C) Raman test patterns of $AlCl_3$ aqueous solutions of different concentrations; and D) charging and discharging curves of the CoHCF electrode in saturated $AlCl_3$ aqueous solution with different charging capacities.

enhancement in the capacity retention rate of the CoHCF electrode.

To illustrate the catalytic effect of CoHCF electrode in the redox process of the Cl^-/Cl^0 pairs, the CV curves of blank collector (Ti mesh), activated carbon (AC, YP-50F) electrode, and CoHCF electrode in saturated $AlCl_3$ aqueous solution were compared (Figure S7, Supporting Information). In the case of titanium mesh as the working electrode, no oxidation peak of Cl^- was detected within the potential range of −0.2–1.1 V (vs SCE) during the forward scanning process. Only when the potential is higher than 1.12 V does the current sharply increase, which corresponds to the oxidation reactions of Cl^- and oxygen evolution. In the case of activated carbon as the working electrode, the current sharply increases when the potential reaches 0.93 V during the forward scanning process, which corresponds to the process of Cl^- oxidation to Cl^0. However, no reduction peak was detected on the CV curve, indicating that the process of reducing Cl^0 to Cl^- on the activated carbon electrode is not easy to occur. For comparison, when CoHCF is used as the working electrode, a pair of redox peaks at high potential can be observed on its CV curve, corresponding to the redox of the Cl^-/Cl^0 pair, which was proved in previous experiments. In addition, during the forward scanning process, when the potential reaches 0.86 V, the current starts to increase sharply, indicating that the oxidation reaction of Cl^- begins at this potential. The above analysis indicates that the order of oxidation activity of Cl^- on several electrodes is: CoHCF > activated carbon > titanium mesh. It is known that activated carbon has a large specific surface area and can adsorb ions or molecules, so the Cl^0 generated after Cl^- oxidation can be adsorbed on its surface. However, no reduction peak was detected on its CV curve, suggesting that the activated carbon has very low catalytic Cl^0 reduction activity. As a control, CoHCF has an efficient catalytic ability for Cl^0 reduction. Therefore, it is concluded that CoHCF can catalyze the redox process of the Cl^-/Cl^0 pairs.

In an effort to explore the energy storage potential of CoHCF electrodes in $AlCl_3$ aqueous solution, we designed an experiment in which several sets of CoHCF electrodes were charged under different charging capacities as cut-off conditions, and then discharged (with a discharge cutoff voltage of −0.2 V vs SCE) to test the changes in their discharge specific capacity. The experimental results show that (Figure 4D) the discharge specific capacity also increases greatly with the increase of charge capacity, which indicates that the above hypothesis is correct. Although the charge capacity can be increased greatly, the

© 2023 Wiley-VCH GmbH

16146840, 2024, 3, Downloaded from https://onlinelibrary.wiley.com/doi/10.1002/aenm.202302712 by University Of Witwatersrand, Wiley Online Library on [02/12/2024]. See the Terms and Conditions (https://onlinelibrary.wiley.com/terms-and-conditions) on Wiley Online Library for rules of use; OA articles are governed by the applicable Creative Commons License

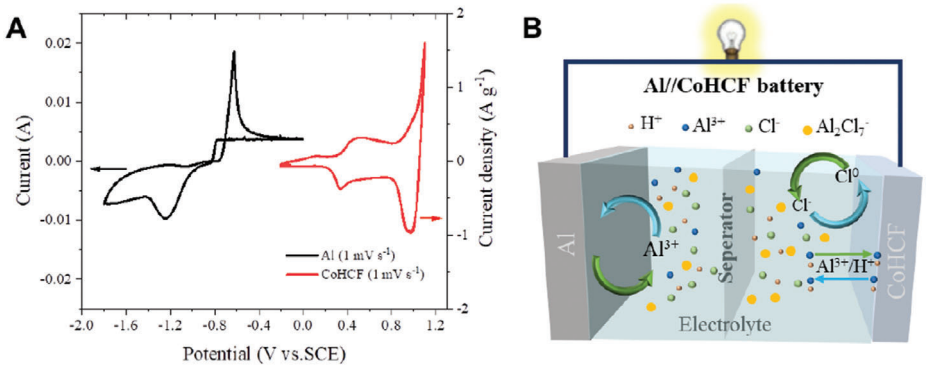

Figure 5. Working principle and CV curves Al//CoHCF battery: A) CV curves of Al and CoHCF electrodes in saturated $AlCl_3$ aqueous solution (1 mV s^{-1}); and B) schematic diagram of working principle of Al//CoHCF battery.

coulombic efficiency is greatly reduced. This may be due to two reasons: 1) the specific surface area and frame space of CoHCF are limited, so when the charge capacity increases, some of the generated Cl° cannot be stored in the host and escapes from the electrode, resulting in a decrease in coulombic efficiency; 2) when the potential is higher than 1.05 V (vs SCE), the side reaction of oxygen evolution becomes more severe, resulting in a decrease in coulombic efficiency. Therefore, considering the long-term cycling stability, practicality, and economic benefits of the battery, the voltage range selection is set according to the single electrode test when a full battery is assembled.

Aluminum can be reversibly deposited and dissolved in ultra-concentrated $AlCl_3$ aqueous solution, as demonstrated in previous studies.[11] The HER (hydrogen evolution reaction) tests conducted in saturated $AlCl_3$ aqueous solution, depicted in Figure S8 (Supporting Information), revealed a hydrogen evolution potential of approximately −1.65 V (vs SCE). This potential is lower than the deposition one of Al^{3+}, indicating the reversible nature of Al^{3+} deposition. Consequently, aluminum can serve as the negative electrode for constructing an ARAIB, as illustrated in **Figure 5A**, with its underlying principle elucidated in Figure 5B. During the charging process, Al^{3+} and a small amount of H^+ are first released from the positive side of CoHCF, and when the potential reaches a higher level, oxidation of Cl^- occurs; on the negative side, Al^{3+} is reduced to Al. During discharge, the sequence reverses. CV test shows that the cell has two redox peaks corresponding to single electrode (Figure S9, Supporting Information). Moreover, when the sweep rate increases to 1 mV s^{-1}, the redox peak is still much obvious, indicating a good rate performance.

The Al//CoHCF full battery not only demonstrates exceptional rate performance but also boasts a high energy density and remarkable cycling stability (**Figure 6**). Under varying current densities of 0.05, 0.25, 0.5, 1, 2, 3, and 4 A g^{-1}, the battery consistently delivers impressive discharge capacities of 103, 92.6, 85.1, 81.9, 72.5, 67.2, 57, and 49.7 mAh g^{-1}, respectively (Figure 6A, B). Furthermore, the Al//CoHCF battery achieves an impressive average discharge voltage of 1.56 V and can attain an energy density up to 155 Wh kg^{-1} (Figure 6C). This energy density significantly surpasses that of most existing aqueous rechargeable batteries, marking a notable advancement in the field of battery technology (Table S3, Supporting Information).[33–37] Al//CoHCF battery also shows excellent cycling performance. At 0.25 A g^{-1} current density, the capacity retention rate reaches 94.7% after 1200 cycles (Figure 6D). The excellent electrochemical performance is mainly attributed to the large framework structure of CoHCF and the high reversibility of Cl^-/Cl^0 redox. In addition, this kind of battery is much safe and environmentally friendly compared with lead-acid battery and nickel cadmium battery, and it will have a great application prospect. From the aforementioned results, it is observed that the Al//CoHCF battery demonstrates outstanding discharge capacities across various current densities, and its energy density and cycling performance are equally impressive. This is mainly attributed to the large framework structure of CoHCF and the high reversibility of the Cl^-/Cl^0 redox couple. Such electrochemical performances, coupled with its relative safety and environmental friendliness, offer immense potential in the realm of energy storage.

3. Conclusions

In summary, we employed a straightforward coprecipitation method to synthesize CoHCF with a nanocube structure, and evaluated its electrochemical performance in saturated $AlCl_3$ aqueous solution. It demonstrated excellent rate performance and cycling stability. Then the energy storage mechanism of CoHCF in saturated $AlCl_3$ aqueous solution was investigated by means of ex-situ XRD. During the charge/discharge cycle, Al^{3+} and a minor amount of H^+ can be seamlessly inserted into and extracted from the CoHCF structure. Furthermore, CoHCF can act as a catalyst, promoting the reversible redox reactions of the Cl^-/Cl^0 pair at elevated potentials, which results in a high specific capacity and redox potential. The assembled Al//CoHCF battery with aluminum as the negative electrode has an average discharge voltage of 1.56 V, and its energy density is up to 155 Wh kg^{-1}. In addition, it exhibits excellent rate and cycling performance. Given its simple material preparation and cost-effectiveness, this ARAIB holds significant promise for energy storage applications.

4. Experimental Section

Synthesis of CoHCF Positive Electrode Material: CoHCF positive electrode material was synthesized by a simple coprecipitation method. In detail, firstly, 0.1 mmol $K_3[Fe(CN)_6]$ (Aladdin) and 0.7 g sodium dodecyl

© 2023 Wiley-VCH GmbH

16146840, 2024, 3, Downloaded from https://onlinelibrary.wiley.com/doi/10.1002/aenm.202302712 by University Of Witwatersrand, Wiley Online Library on [02/12/2024]. See the Terms and Conditions (https://onlinelibrary.wiley.com/terms-and-conditions) on Wiley Online Library for rules of use; OA articles are governed by the applicable Creative Commons License

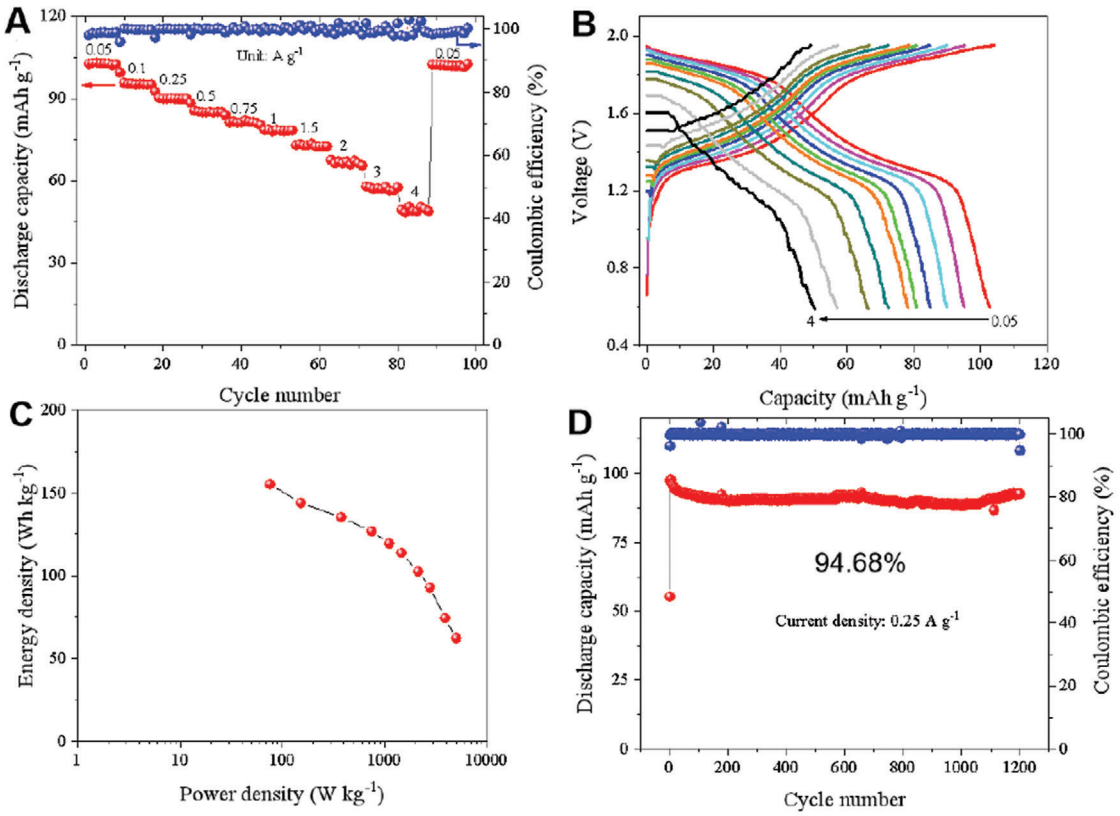

Figure 6. Electrochemical performance tests of Al//CoHCF batteries: A) Capacities at different current densities; B) charge-discharge curves at different current densities; C) change of energy density with power one; and D) cycling at a current density of 0.25 A g^{-1}.

sulfate (SDS) (Aladdin) were dissolved in 20 mL DI water to achieve solution A. Then, 0.2 mmol $Co(CH_3COO)_2{\cdot}4H_2O$ (Aladdin) was dissolved into 20 mL DI water to obtain solution B. After that, solution B was slowly added into solution A to form a mixture which was subsequently aged in ambient environment for 24 h. The resulted earthy yellow precipitates were then collected by centrifugation and repeatedly washed with DI water and ethanol for three times. Finally, the resulting product was dried overnight in a vacuum oven at 80 °C.

Characterization: X-ray diffraction (XRD) patterns were collected on a model Rigaku Smart Lab TM diffractometer using a Cu Kα (1.5406 Å) radiation source operating at a voltage of 40 kV and a current of 40 mA. Scanning electron microscopy (SEM) images and energy dispersive X-ray spectroscopy (EDS) spectra were obtained from a field emission scanning electron microscope (FESEM, JEOL, JSM-7800F). Inductively coupled plasma emission spectroscopy (ICP-OES) analysis was performed using Prodigy full spectrum direct reading emission spectrometer. The samples submitted to different charging and discharging conditions were cleaned with water and ethanol and dried, and then characterized by ex situ XRD to analyze the crystal changes of the samples during the charging and discharging processes.

Electrochemical Measurements: The positive electrodes were prepared by mixing active materials, acetylene black, and poly(tetrafluoroethylene) (PTFE) with a weight ratio of 7:2:1. The homogeneous slurries with the mass loading of 10 mg cm^{-2} were cast onto titanium mesh current collectors and dried under vacuum. After drying, they were cut into discs for use. The single-electrode performance test was conducted using a three-electrode system, with titanium mesh as the counter electrode and saturated calomel electrode (SCE) as the reference electrode. The full batteries were assembled using dual electrolytic cells. The electrolytes used in this work include saturated $Al_2(SO_4)_3$ and various concentrations of $AlCl_3$ aqueous solutions. For electrochemical performance testing, the operating voltage range of single electrode was set to −0.2_1.05 V (vs SCE), and the operating voltage range of the whole battery was fixed in the range of 0.6–1.95 V. Cyclic voltammetry (CV) and the electrochemical impedance measurements (EIS) were carried out using CHI 660C electrochemical work station. EIS data was recorded from 10^5 to 0.01 Hz with an amplitude of 10 mV. All electrochemical tests were performed at room temperature.

Supporting Information

Supporting Information is available from the Wiley Online Library or from the author.

Acknowledgements

Financial support of National Key R & D Program of China for Young Scholars (2022YFB2404600), NSFC Key Project (52131306 and 52122209), Project on Carbon Emission Peak and Neutrality of Jiangsu Province (BE2022031-4) is gratefully acknowledged. The authors acknowledge the support of the DSI-NRF-WITS SARChI Chair in Materials Electrochemistry and Energy Technologies (MEET) (UID No. 132739).

Conflict of Interest

The authors declare no conflict of interest.

Data Availability Statement

The data that support the findings of this study are available on request from the corresponding author. The data are not publicly available due to privacy or ethical restrictions.

© 2023 Wiley-VCH GmbH

16146840, 2024, 3, Downloaded from https://onlinelibrary.wiley.com/doi/10.1002/aenm.202302712 by University Of Witwatersrand, Wiley Online Library on [02/12/2024]. See the Terms and Conditions (https://onlinelibrary.wiley.com/terms-and-conditions) on Wiley Online Library for rules of use; OA articles are governed by the applicable Creative Commons License

Keywords

Al metal, aqueous rechargeable Al-ion battery, cobalt hexacyanoferrate, high energy density

Received: August 17, 2023
Revised: October 18, 2023
Published online: November 29, 2023

[1] M.-C. Lin, M. Gong, B. Lu, Y. Wu, D.-Y. Wang, M. Guan, M. Angell, C. Chen, J. Yang, B.-J. Hwang, H. Dai, *Nature* **2015**, *520*, 324.
[2] T. H. Cai, L. M. Zhao, H. Y. Hu, T. G. Li, X. C. Li, S. Guo, Y. P. Li, Q. Z. Xue, W. Xing, Z. Yan, L. Wang, *Energy Environ. Sci.* **2018**, *11*, 2341.
[3] L. Miao, Z. Guo, L. Jiao, *Energy Mater.* **2023**, *3*, 300014.
[4] H. J. Zhou, G. Y. Zhu, S. Y. Dong, P. Liu, Y. Y. Lu, Z. Zhou, S. Cao, Y. Z. Zhang, H. Pang, *Adv. Mater.* **2023**, *35*, 22115.
[5] T. Lv, G. Zhu, S. Dong, Q. Kong, Y. Peng, S. Jiang, G. Zhang, Z. Yang, S. Yang, X. Dong, H. Pang, Y. Zhang, *Angew. Chem., Int. Ed.* **2023**, *62*, e202216089.
[6] F. Ambroz, T. J. Macdonald, T. Nann, *Adv. Energy Mater.* **2017**, *7*, 1602093.
[7] H. Jia, Z. Wang, B. Tawiah, Y. Wang, C.-Y. Chan, B. Fei, F. Pan, *Nano Energy* **2020**, *70*, 104523.
[8] J. B. Goodenough, K.-S. Park, *J. Am. Chem. Soc.* **2013**, *135*, 1167.
[9] D. Yuan, W. Manalastas Jr, S. Kumar, M. Srinivasan, *Nano Mater. Sci.* **2020**, *2*, 248.
[10] G. A. Elia, K. Marquardt, K. Hoeppner, S. Fantini, R. Lin, E. Knipping, W. Peters, J.-F. Drillet, S. Passerini, R. Hahn, *Adv. Mater.* **2016**, *28*, 7564.
[11] W. Pan, Y. Wang, Y. Zhang, H. Y. H. Kwok, M. Wu, X. Zhao, D. Y. C. Leung, *J. Mater. Chem. A* **2019**, *7*, 17420.
[12] H. Lahan, A. Hazarika, S. K. Das, *J. Phys. Chem. C* **2017**, *121*, 26241.
[13] T. Dong, K. L. Ng, Y. Wang, O. Voznyy, G. Azimi, *Adv. Energy Mater.* **2021**, *11*, 2100077.
[14] X. Yuan, F. Ma, L. Zuo, J. Wang, N. Yu, Y. Chen, Y. Zhu, Q. Huang, R. Holze, Y. Wu, T. Van Ree, *Electrochem. Energy Rev.* **2021**, *4*, 1.
[15] C. Yan, C. Lv, B.-E. Jia, L. Zhong, X. Cao, X. Guo, H. Liu, W. Xu, D. Liu, L. Yang, J. Liu, H. H. Hng, W. Chen, L. Song, S. Li, Z. Liu, Q. Yan, G. Yu, *J. Am. Chem. Soc.* **2022**, *25*, 11444.
[16] G. R. Pastel, Y. Chen, T. P. Pollard, M. A. Schroeder, M. E. Bowden, A. Zheng, N. T. Hahn, L. Ma, V. Murugesan, J. Ho, M. Garaga, O. Borodin, K. Mueller, S. Greenbaum, K. Xu, *Energy Environ. Sci.* **2022**, *15*, 2460.
[17] Q. Zhao, M. J. Zachman, W. I. Al Sadat, J. Zheng, L. F. Kourkoutis, L. Archer, *Sci. Adv.* **2018**, *4*, eaau8131.
[18] S. He, J. Wang, X. Zhang, J. Chen, Z. Wang, T. Yang, Z. Liu, Y. Liang, B. Wang, S. Liu, L. Zhang, J. Huang, J. Huang, L. A. O'dell, H. Yu, *Adv. Funct. Mater.* **2019**, *29*, 1905228.
[19] Z. Li, K. Xiang, W. Xing, W. C. Carter, Y.-M. Chiang, *Adv. Energy Mater.* **2015**, *5*, 1401410.
[20] S. Liu, G. L. Pan, G. R. Li, X. P. Gao, *J. Mater. Chem. A* **2015**, *3*, 959.
[21] J. Wang, L. Zhang, L. Yu, Z. Jiao, H. Xie, X. W. Lou, X. Wei Sun, *Nat. Commun.* **2014**, *5*, 4921.
[22] A. Zhou, L. Jiang, J. Yue, Y. Tong, Q. Zhang, Z. Lin, B. Liu, C. Wu, L. suo, Y. S. Hu, H. Li, L. Chen, *ACS Appl. Mater. Interfaces* **2019**, *11*, 41356.
[23] C. Wu, S. Gu, Q. Zhang, Y. Bai, M. Li, Y. Yuan, H. Wang, X. Liu, Y. Yuan, N. Zhu, F. Wu, H. Li, L. Gu, J. Lu, *Nat. Commun.* **2019**, *10*, 73.
[24] L. Ma, S. Chen, C. Long, X. Li, Y. Zhao, Z. Liu, Z. Huang, B. Dong, J. A. Zapien, C. Zhi, *Adv. Energy Mater.* **2019**, *9*, 1902446.
[25] L. Ma, X. Li, G. Zhang, Z. Huang, C. Han, H. Li, Z. Tang, C. Zhi, *Energy Storage Mater.* **2020**, *31*, 451.
[26] X. Wu, C. Wu, C. Wei, L. Hu, J. Qian, Y. Cao, X. Ai, J. Wang, H. Yang, *ACS Appl. Mater. Interfaces* **2016**, *8*, 5393.
[27] C. Li, W. Yan, S. Liang, P. Wang, J. Wang, L. Fu, Y. Zhu, Y. Chen, Y. Wu, W. Huang, *Nanoscale Horiz.* **2019**, *4*, 991.
[28] Q. Yang, F. Mo, Z. Liu, L. Ma, X. Li, D. Fang, S. Chen, S. Zhang, C. Zhi, *Adv. Mater.* **2019**, *31*, 1901521.
[29] X. Wu, Y. Qi, J. J. Hong, Z. Li, A. S. Hernandez, X. Ji, *Angew. Chem., Int. Ed. Engl.* **2017**, *56*, 13026.
[30] X. Yuan, F. Ma, X. Chen, R. Sun, Y. Chen, L. Fu, Y. Zhu, L. Liu, F. Yu, J. Wang, Y. Wu, *Mater. Today Energy* **2021**, *20*, 100660.
[31] X. Zhao, Y. Wang, Y. Shi, X. Yan, Y. Tian, Z. Zuo, X. Yang, *ACS Energy Lett.* **2021**, *6*, 1134.
[32] Y. Sui, M. Lei, M. Yu, A. Scida, S. K. Sandstrom, W. Stickle, T. D. O'larey, D.-E. Jiang, X. Ji, *ACS Energy Lett.* **2023**, *8*, 988.
[33] L.-P. Wang, P.-F. Wang, T.-S. Wang, Y.-X. Yin, Y.-G. Guo, C.-R. Wang, *J. Power Sources* **2017**, *355*, 18.
[34] S. Gheytani, Y. Liang, F. Wu, Y. Jing, H. Dong, K. K. Rao, X. Chi, F. Fang, Y. Yao, *Adv. Sci.* **2017**, *4*, 1700465.
[35] Y. Liu, Z. Wen, X. Wu, X. Wang, Y. Wu, R. Holze, *Chem. Commun.* **2014**, *50*, 13714.
[36] Y. Liu, B. H. Zhang, X. W. Wu, Y. Q. Yang, Z. Chang, Z. B. Wen, Y. P. Wu, *Chem. Commun.* **2014**, *50*, 1209.
[37] X. Zhang, X. Zhang, Y. Miao, Q. Huang, Z. Chen, D. Guo, J. Xu, Y.-M. Shen, J. Cao, *J. Mater. Chem. A* **2023**, *11*, 7152.

© 2023 Wiley-VCH GmbH

16146840, 2024, 3, Downloaded from https://onlinelibrary.wiley.com/doi/10.1002/aenm.202302712 by University Of Witwatersrand, Wiley Online Library on [02/12/2024]. See the Terms and Conditions (https://onlinelibrary.wiley.com/terms-and-conditions) on Wiley Online Library for rules of use; OA articles are governed by the applicable Creative Commons License